A discrete-time localization method for capsule endoscopy based on on-board magnetic

sensing

A discrete-time localization method for capsule endoscopy based on on-board magnetic sensing

Marco Salerno[1]**, Gastone Ciuti**[1]**, Gioia Lucarini**[1]**, Rocco Rizzo**[2]**,
Pietro Valdastri**[1,3]**, Arianna Menciassi**[1]**, Alberto Landi**[2] **and Paolo Dario**[1]

[1] Scuola Superiore Sant'Anna—The BioRobotics Institute, P.za Martiri della Liberta' 33, 56127 PISA, Italy
[2] Department of Electric Systems and Automation, University of Pisa, via Diotisalvi 2, 56126 PISA, Italy

E-mail: m.salerno@sssup.it

Abstract

Recent achievements in active capsule endoscopy have allowed controlled inspection of the bowel by magnetic guidance. Capsule localization represents an important enabling technology for such kinds of platforms. In this paper, the authors present a localization method, applied as first step in time-discrete capsule position detection, that is useful for establishing a magnetic link at the beginning of an endoscopic procedure or for re-linking the capsule in the case of loss due to locomotion. The novelty of this approach consists in using magnetic sensors on board the capsule whose output is combined with pre-calculated magnetic field analytical model solutions. A magnetic field triangulation algorithm is used for obtaining the position of the capsule inside the gastrointestinal tract. Experimental validation has demonstrated that the proposed procedure is stable, accurate and has a wide localization range in a volume of about 18×10^3 cm^3. Position errors of 14 mm along the X direction, 11 mm along the Y direction and 19 mm along the Z direction were obtained in less than 27 s of elaboration time. The proposed approach, being compatible with magnetic fields used for locomotion, can be easily extended to other platforms for active capsule endoscopy.

Keywords: capsule endoscopy, magnetic field model, magnetic localization

(Some figures in this article are in colour only in the electronic version)

1. Introduction

Wireless capsule endoscopy (WCE) is progressively emerging as an effective non-invasive tool for gastrointestinal (GI) tract screening [1]. In particular, WCE, provided with active locomotion, allows the endoscopist to guide and steer the capsule. This feature could lead to obtaining the same reliability as with traditional flexible endoscopy, but with much less pain for the patient.

Accordingly, many research groups are working to develop active locomotion devices and platforms [2–4]. A
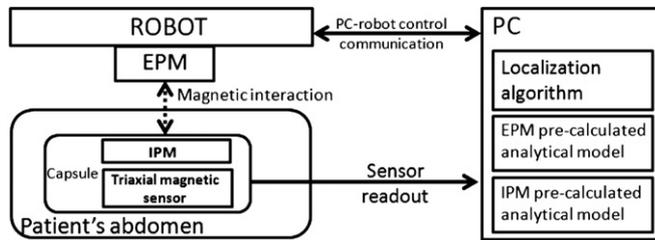
promising approach for active locomotion is to magnetically control endoscopic capsules by means of external magnetic fields, thus overcoming powering issues [5–13].

A significant issue for capsule endoscopy teleoperated procedures is knowing where the device is positioned during GI tract examination. The most common localization strategies operate in different manners: through radio frequency signals emitted by the capsule and measured by antennas placed outside the abdomen [14–16], by magnetic tracking of a permanent magnet placed inside the capsule using external magnetic sensors [11, 13, 17–19] or by localizing a magnetic sensor inside the capsule using external magnetic field sources [20, 21]. In particular, a localization strategy that suits with magnetic actuation in spiral motion has been

---

[3] Present address: STORM Lab, Department of Mechanical Engineering, Vanderbilt University, Nashville, TN, USA.

Table 1. Geometric and magnetic characteristics of the PMs. B_{rem} and H_c represent the remanence and the coercivity of magnets, respectively.

PM	Magnetization	Material	B_{rem} (T)	H_c (A m^{-1})	R_{in} (mm)	R_{out} (mm)	h (mm)
EPM	Diametral	NdFeB	1.21	9.63×10^5	5	30	70
IPM	Axial	NdFeB	1.48	11.78×10^5	0	1.6	19.2

Figure 1. Diagram of the platform components involved in the localization procedure.

proposed by [21] where magnetic field information is obtained by the external rotating magnet used for locomotion.

An innovative approach, based on magnetic sensing and compatible with magnetic driven slide motion, is described in this paper. The proposed localization procedure, currently implemented as automatic but discrete-time, is based on pre-calculated magnetic field models and a triangulation algorithm which determines the position of the capsule inside the GI tract. The magnetic field magnitude is acquired by placing a triaxial magnetic sensor inside the capsule and the position of the capsule is determined based on the intersection point of analytically pre-calculated iso-value surfaces of magnetic field.

In order to apply and validate the proposed procedure, a robotic platform previously developed by the authors was used [8]. The platform is composed of a six degrees of freedom (DOFs) anthropomorphic robotic arm equipped with an external permanent magnet (EPM). Control of the robotic arm allows accurate movement and orientation of a capsule embedding an internal permanent magnet (IPM). This robotic platform, schematically represented in figure 1, was used for localizing the endoscopic capsule inside the human body, thus establishing a magnetic link at the beginning of an endoscopic procedure or re-linking the capsule in the case of loss. Although this approach was implemented and applied to a specific endoscopic platform, it can be extended to platforms exploiting magnetic field sources for active locomotion in capsule endoscopy, such as the one presented in [22] by the main industrial players in the field of medical devices.

2. Magnetic field model

In order to implement the proposed procedure, an analytical magnetic field model of the EPM, fixed onto the robotic arm, and of the IPM, on board the capsule, was developed.

2.1. Theoretical basis and applied model

Two different methods may be used for analyzing the magnetic field produced by permanent magnets (PMs). The first, named 'current model', is based on the equivalent current

distribution, while the second, named 'the charge model', uses the equivalent magnetic charge distribution. Both distributions, properly positioned in space, are able to produce the same magnetic field as the original PM system [23]. From a practical viewpoint, if the whole region of interest does not contain free or displacement currents (i.e. $\nabla \times \boldsymbol{H} = 0$), the two models give the same result. The charge model is used in this paper.

The referenced formulation was applied to find the magnetic induction $\boldsymbol{B}$ produced by the permanent magnet fixed on the robotic arm (EPM) and by the magnet on board the capsule (IPM). The EPM is a hollow cylinder with given inner and outer radius and height, and permanently magnetized along the diametral direction. The IPM, instead, is composed by three solid cylinders with magnetization along their axial direction. Table 1 summarizes the main characteristics of these two systems.

As regards the EPM, since its relative permeability is approximately equal to the permeability of air ($\mu_r \simeq 1$) and since the environment does not contain ferromagnetic materials, it could be analyzed by superimposing two different solutions [24] as shown in figure 2.

The original system could be split into two solid cylinders with radius respectively equal to the outer and inner radius of the hollow cylinder. Since the two problems differ only in the value of the radius and in the magnetization sign, they have similar solutions. In a cylindrical coordinate system $\xi = (r, \varphi, z)$, the complete solution for the hollowed cylinder is the difference between the magnetic field due to problems a and b: $\boldsymbol{B}_P(\xi_P) = \boldsymbol{B}_{P_a}(\xi_P) - \boldsymbol{B}_{P_b}(\xi_P)$. A similar analysis leads to the equations for the magnetic field produced by the IPM magnetized along the z-direction. By taking into account the physical and geometrical symmetry of the system whereby $B_\varphi(r, \varphi, z) = 0$, it is possible to obtain the field in a generic point $P(r, \varphi, z)$ of space. The integrations in [25] and [26] were performed by using Simpson's method implemented in the MATLAB (Mathworks, Inc., USA) routines used.

2.2. Permanent magnet coupling effects

In the endoscopic platform of figure 1, magnetic locomotion is based on EPM and IPM interaction. Diametral magnetized EPMs, axial magnetized IPMs and magnet position design have been evaluated and verified in [8] to allow capsule pitch and yaw rotations and forward–backward translation. Since the sensors used for magnetic field measurements are placed inside the capsule, the IPM effect on them has to be analyzed. As explained in section 2.1, the solution for the hollow cylinder may be obtained by superimposing two different solutions, just as the magnetic field resulting from two or more magnets may be obtained by exploiting the superimposition effects
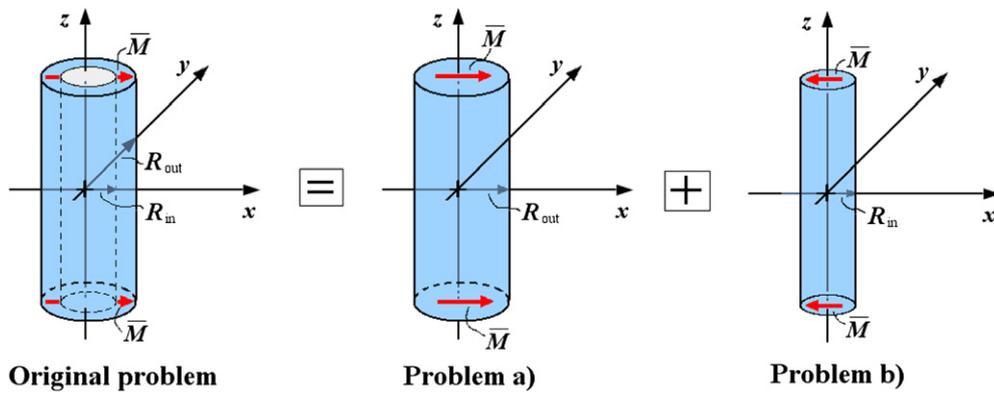
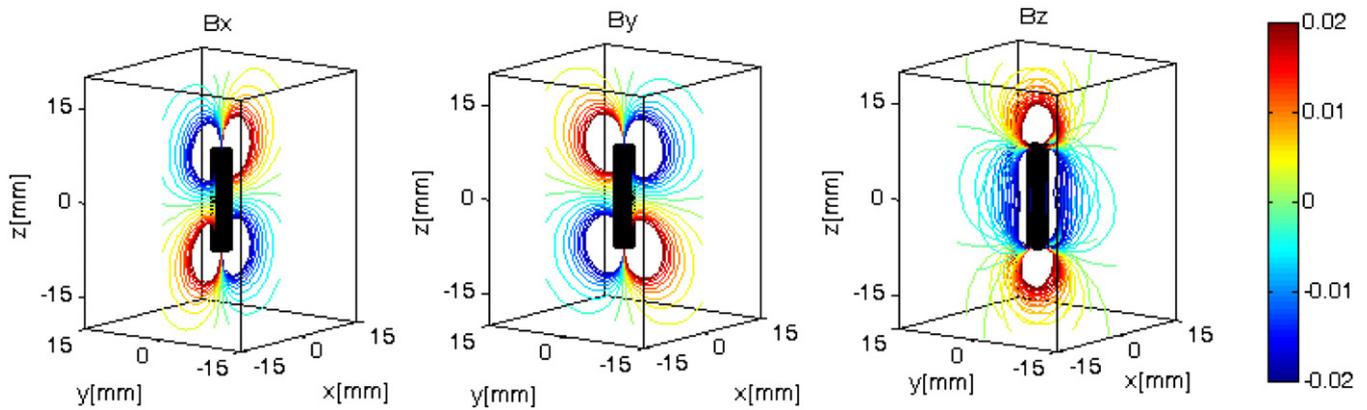**Figure 2.** The EPM system and the superimposed solutions.

Figure 3. IPM magnetic field model solution used to minimize the IPM effect on sensors. Left: axially magnetized single column solution, contour of the magnetic field X component in the $Y = 0$ plane. Center: contour of the magnetic field Y component in the $X = 0$ plane. Right: contour of the magnetic field Z component in the $X = 0$ and $Y = 0$ planes, color bar in tesla.

(if the environment does not contain ferromagnetic materials). The validation of the EPM magnetic field model may also be considered as the validation of the superimposition effects. The analytical results coming from a subtraction of the two solutions will be experimentally validated in section 2.3. In the proposed platform, the position of the sensors in relation to the IPM is fixed since both are on board the capsule. This allows the IPM effect to be considered as an offset on sensor readout. In order to overcome sensor range limitations due to this offset, a wide range sensor (0.2 mT–2 T) has been selected. To minimize the IPM effect on sensor output, their relative position was defined exploiting the IPM magnetic field model solution. In order to place the sensors correctly, the plane $Z = 0$ was selected in which only the Z magnetic field component is different from zero (figure 3); however, the sensor relative to the Z direction does not reach saturation level due to its wide measurement range. As shown in figure 5, the sensor has been placed centering its origin in the $Z = 0$ plane of the IPM.

2.3. Model validation

The developed analytical magnetic model was validated both numerically and experimentally. A first preliminary validation was carried out by comparing the analytical solutions with numerical simulations obtained by a finite-element method (FEM) code developed at the University of Bath (UK) (MEGA

2001). For brevity, the comparison will not be examined in this paper, but maximum error is below 5%, showing good agreement between analytical and numerical results.

A more in-depth experimental validation was performed using the platform sketched in figure 1 with a monoaxial magnetic sensor instead of the capsule. The robotic arm (RV-3SB Mitsubishi Electric, Japan) was used to hold, accurately move and orient the EPM. The permanent magnets are those described in table 1, while a monoaxial Hall effect sensor (SS94A2, Honeywell, Morristown, USA) with 50 mV mT^{-1} sensitivity and high signal-to-noise ratio was used to measure the actual magnetic field. The sensor was interfaced to a National Instruments data acquisition board (NI USB-6259, National Instruments, Inc., USA) and the signal was elaborated in real time with a dedicated program developed with LabVIEW (National Instruments, Inc., USA). Finally, an elaboration routine was implemented with MATLAB to compare analytical and experimental results. The monoaxial magnetic sensor was fixed in reference positions with respect to the magnetic source. Then, the EPM was moved by the robot arm along specific directions and the magnetic field values were recorded with 5 mm steps for the EPM and 0.5 mm steps for the IPM. Adequate alignment between the sensor and the magnetic module was verified based upon the knowledge of the magnetic field symmetries and sensor outputs. The sets of measurements were repeated in order
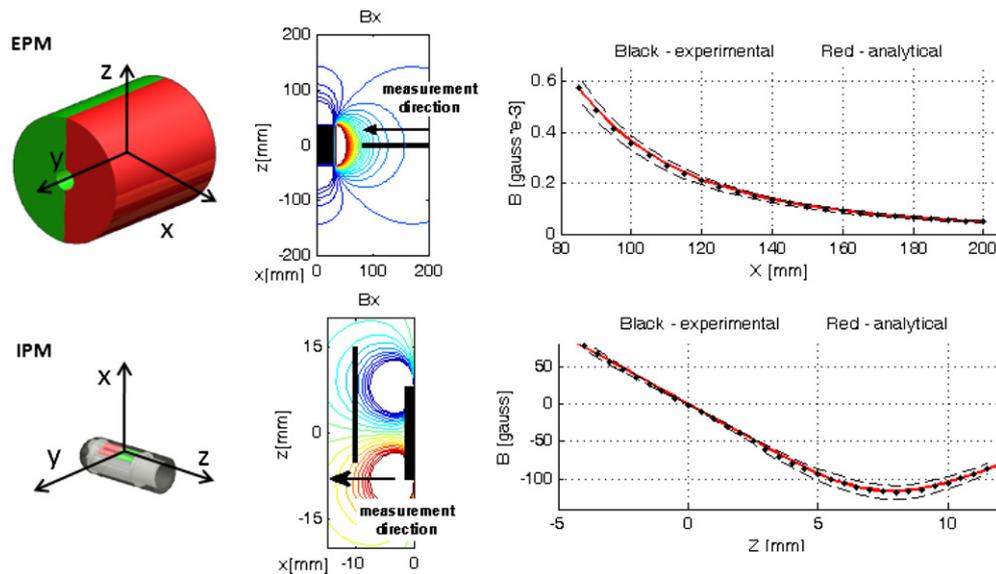
Figure 4. EPM in the upper line, IPM in the lower. From left to right: reference system, relative position between the sensor and the magnet with the measuring line and moving direction superimposed to the magnetic field map, comparison between experimental measurements (black dots), measurement uncertainty (black dashed line) and analytical model (red line).

to obtain different magnetic field components, both for the diametrically magnetized external magnet and for the internal axially magnetized magnets (figure 4).

Typical screenshots of the comparison analysis are reported in figure 4, respectively, for the EPM and IPM. In this case, the maximum error between the calculated magnetic field and the experimental measurements is below 0.8%, showing high analytical model performances.

3. The proposed localization procedure

The goal of the proposed work is to develop a reliable discrete-time localization algorithm capable of detecting the position of the magnetic capsule in the patient's GI tract during a robotic-aided active diagnostic examination. This is fundamental for establishing the magnetic link, especially at the beginning of the procedure or in the case of capsule loss. The localization method is based on a triangulation process of magnetic field measurements matched with planned translational movements of the EPM and with pre-calculated analytical models, thus minimizing computational complexity.

A triaxial magnetic sensor on board the capsule measures the magnetic field produced by the EPM fixed in predefined positions in space. Then, as detailed in section 3.3, an intersection procedure is employed, using the measured and calculated magnetic field values, in order to obtain the relative position between the EPM and the capsule.

3.1. The set-up

The equipment used to implement and validate the localization procedure comprises an endoscopic capsule, including the IPM and the on-board triaxial magnetic sensor, and a robotic arm to control the EPM position (figure 1). In particular, the IPM is composed of three solid cylinders with magnetization along its axial direction. The three magnets are arranged symmetrically to the middle longitudinal plane of the capsule and arranged

close to the external shell of the capsule, thus providing always the same orientation of the camera, once coupled with the EPM. The endoscopic capsule (figure 5) has a diameter of 16.5 mm, length 46.5 mm and weight 18.4 g. The vision system consists of a wired complementary metal oxide semiconductor (CMOS) camera (MO-S88-3T-N, Misumi Manufacturer & Exporter, Taiwan) and an illumination module (four white light emitting diodes). The magnetic internal module is composed of three neodymium N52 cylindrical magnets whose geometric and magnetic characteristics are reported in table 1 (K&J Magnetics, Inc., USA). As regards the magnetic sensor, since a suitable product working in the requested range was unavailable, a custom triaxial sensor was developed. Three mono-axial commercially available sensors with a measuring range from 0.1 μT to 2T (Hall Effect Sensor CY-P15A, Chen Yang Technologies GmbH & Co. KG) were assembled on the three perpendicular directions. In particular, the sensors were fixed on the three faces of a 5 mm side polymeric cube (figures 5(*c*) and (*d*)). The sensor outputs were processed and amplified (AD620 instrumentation amplifier, Analog Devices, MD, USA) by a custom electronic board.

The sensor was connected to the data acquisition board and the signal was elaborated in real time with software developed in LabVIEW.

3.2. Operating conditions

In order to obtain reliable implementation of the localization strategy, the EPM has to be far enough from the capsule, thus limiting significant interaction forces during the measurement (i.e. the capsule should not be lifted by the EPM). On the other hand, the EPM and capsule should be close enough to allow accurate magnetic field measurements by the on-board magnetic sensors. In order to define the localization operating range, an experimental test was performed. The capsule was
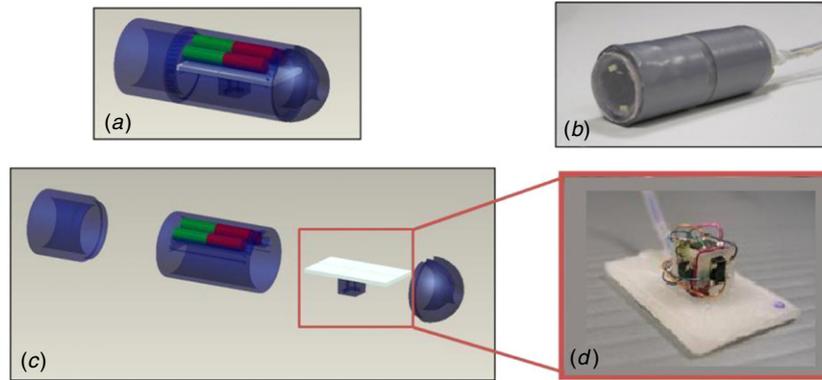
Figure 5. (*a*) The assembled model of the endoscopic capsule, (*b*) the capsule prototype, (*c*) the exploded capsule model and (*d*) the custom triaxial sensor.
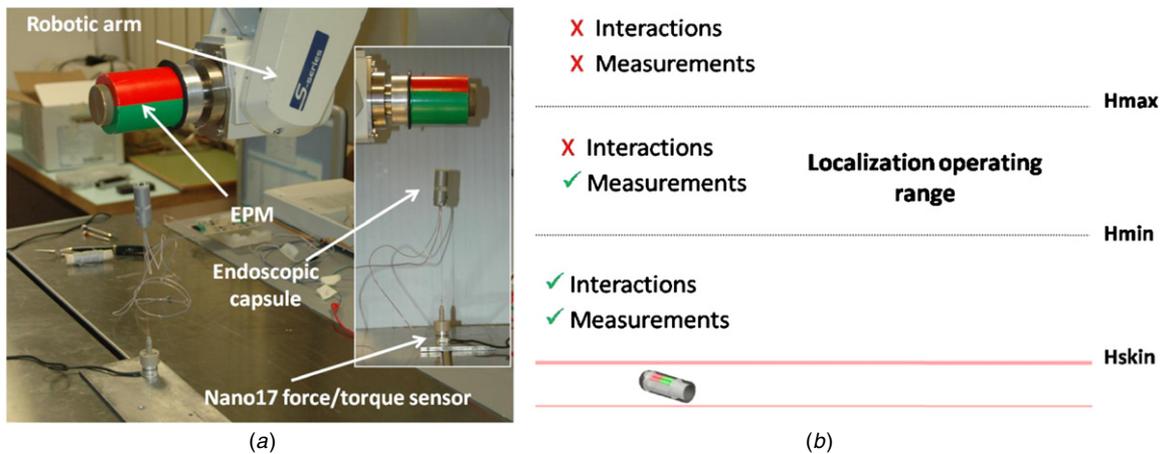

Figure 6. (*a*) Experimental set-up arranged for defining the localization operating range. (*b*) Operating ranges defined thanks to the test bench.

fixed to a triaxial force/torque sensor (Nano17, ATI Industrial Automation, USA) and positioned in contact with the EPM. The EPM was moved away from the capsule (range from 0 to 250 mm) by means of the robotic system. The attraction force and the magnetic field were measured by a 1 mm incremental step, up to the capsule attraction limit. As this limit was exceeded, the magnetic field was measured in steps of 5 mm (figure 6(*a*)).

As reported in figure 6(*b*), it was possible to define three operating ranges: the first, where the EPM magnetic field can be measured by the sensors and the capsule is attracted and lifted by the magnetic field; the second, where magnetic forces between EPM and IPM are not high enough to lift the capsule and the EPM magnetic field can be measured by the sensors; the last, where both localization measurements and interaction forces are negligible. The lower limit of the localization measurement range (Hmin) was defined as the maximum EPM-capsule distance where magnetic attraction force balances the capsule weight. The upper limit (Hmax) was found as the maximum distance where the magnetic field module, measured by the sensor, records a value equal to 2.5 mT (i.e. sensor magnetic field threshold providing information within an acceptable 10% error).

Consequently, the best operating EPM-capsule distance for the sake of localization can be defined as the distance between the capsule and the middle point of the localization operating range (level 0). The three ranges are numerically defined upon experimental evidence, as reported in section 4.

These operative ranges are affected by changes of the capsule weight or magnetization. An increase in capsule weight expands the localization range and lowers the attraction limit (Hmin), while an increase in IPM magnetic features (i.e. volume or magnetization) reduces the operative range and makes the attraction limit (Hmin) rise. Due to the high variability of abdominal wall thickness [27] and GI tract size, an accurate model for Hmin and Hmax evaluation would be of limited use for the proposed application. To overcome these problems, the employment of wide dynamic range sensors would allow an increased operative range.

3.3. Description of the localization procedure

The localization procedure, based on triangulation methodology, consisted of three iterative steps, as follows:

(i) placing the external magnet, mounted on the robot, in a position above the patient's abdomen;
(ii) measuring the external magnetic field module through the triaxial magnetic field sensor placed on board the capsule;
(iii) obtaining, from the pre-calculated analytical EPM model in MATLAB, the cloud of points with a magnetic field module as measured in the previous step.
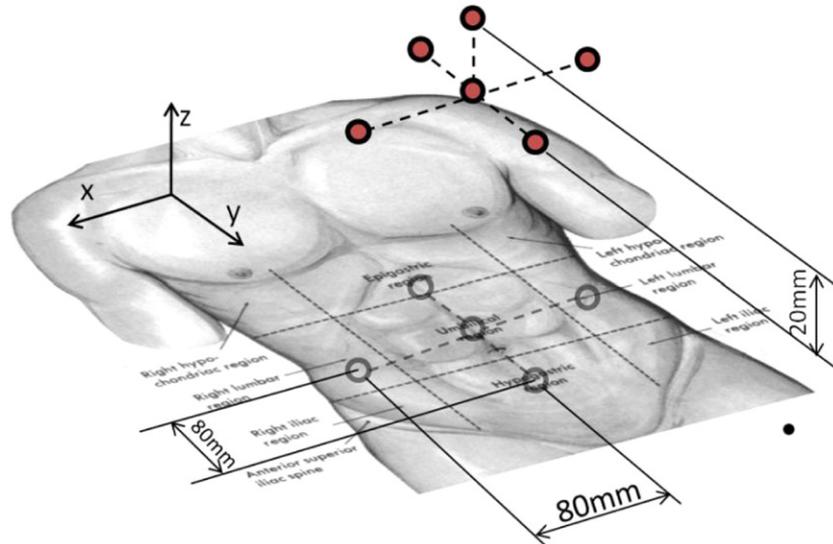
Figure 7. Localization procedure measurements above the abdominal area.

The EPM positions were standardized in order to optimize measurement quality independently on the capsule position in the GI tract. In particular, six measurements were performed as shown in figure 7.

After performing the six measurements, we consider at least three of these measurements (the selection method is reported below); thus, the position of the capsule with respect to the EPM can be defined as the intersection of the calculated iso-magnetic field module clouds of points (figure 8). Finally, the EPM is moved to the new calculated point in the *XY* plane and then the magnet is brought down along the *Z* axis until the capsule is attracted.

In order to define which measurements have to be considered in the intersection of the clouds, four different algorithms with varying parameters were implemented and tested. Some algorithms were based on the triangulation principle, while others were built upon a variable number of measurements exceeding a pre-defined magnetic field threshold level. The first algorithm considered the three highest measurements, while the second algorithm based its choice on the magnetic field module threshold (2.5 mT), i.e. if three or more values were above the threshold, it considered the three highest measurements; otherwise it considered the four highest ones. The number of measurements considered in the second algorithm was varied by producing 15 different combinations. The third and fourth algorithms were defined by taking into account the triangulation theory. The third algorithm considered the two central measurements, the maximum lateral measurement and the maximum measurement between superior and inferior, while the fourth algorithm considered the maximum central measurement, the maximum lateral measurement and the maximum measurement between superior and inferior. Furthermore, a parameter regulating cloud thickness was automatically defined in each elaboration by a MATLAB routine in order to consider sensor readout errors and small capsule motions caused by minimal magnetic interactions or by physiological movements of the abdomen. Regarding the

intersection of iso-magnetic field module clouds of points, a simple algorithm based on pre-calculated magnetic field values can be set up through search and sort functions. The pre-calculated magnetic field map (*Bmap*) is loaded into a matrix organized as a list of *n* coordinates that discretize the domain (in the EPM reference system) with the relative magnetic field module. The input matrix (*Bloc*) is organized as a list of predefined EPM position deviations (figure 7) with the relative measured magnetic field module. Surfaces and intersections of surfaces are described by matrices organized as a list of coordinates. In case the intersection function returns an empty matrix due to volume discretization or noise in sensor readout, the interaction of clouds of points is assured by a parameter that increases surface thickness (*thick*) at each iteration; as an example, the cloud intersection pseudocode in the case of three measurements is as follows:

$$Bmap = \begin{bmatrix} x_1 & y_1 & z_1 & |B|_1 \\ \vdots & \vdots & \vdots & \vdots \\ x_n & y_n & z_n & |B|_n \end{bmatrix};$$

$$Bloc = \begin{bmatrix} \mathrm{d}x_1 & \mathrm{d}y_1 & \mathrm{d}z_1 & |B|_1 \\ \mathrm{d}x_2 & \mathrm{d}y_2 & \mathrm{d}z_2 & |B|_2 \\ \mathrm{d}x_3 & \mathrm{d}y_3 & \mathrm{d}z_3 & |B|_3 \end{bmatrix}.$$

Surface intersection algorithm pseudocode:

increasethick = 1;
thick = 0;
while *increasethick* == 1 **do**
   thick = *thick* + 0.01;
   for *k* = 1 → 3 **do**
    idxsurf = *find* ((*Bloc*(*k*, 4) *(1 − *thick*)) ⩽ *Bmap*(:,4) ⩽ (*Bloc*(*k*, 4) *(1+ *thick*)));
    surface(*k*) = *Bmap*(*idxsurf*, 1:3) + *Bloc*(*k*, 1:3);
   end for
   *intersection*12 = *intersect* (*surface*(1), *surface*(2),′ *rows*′);
   *intersection*123 = *intersect*(*intersection*12, *surface*(3),′ *rows*′);
   if *isempty* (*intersection*123) == 0 **then**
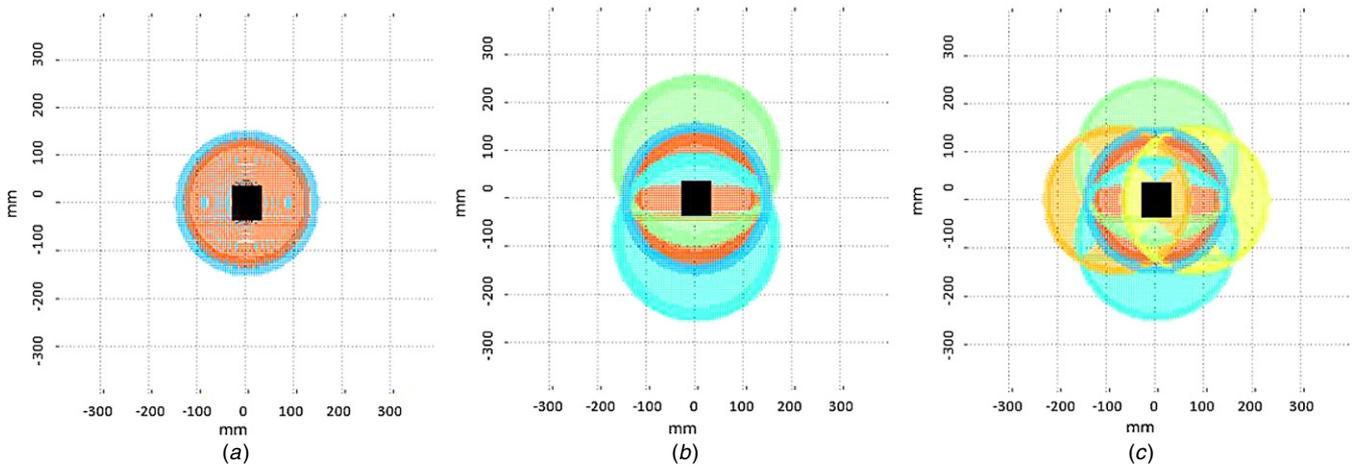   *increasethick* = 0;

Figure 8. Intersection of the calculated iso-magnetic field module clouds of points for defining the *XYZ* position of the capsule with respect to the EPM. (*a*) First two measurements above the umbilical region along the *Z* axis, (*b*) second two measurements along the *X* axis and (*c*) last two measurements along the *Y* axis.
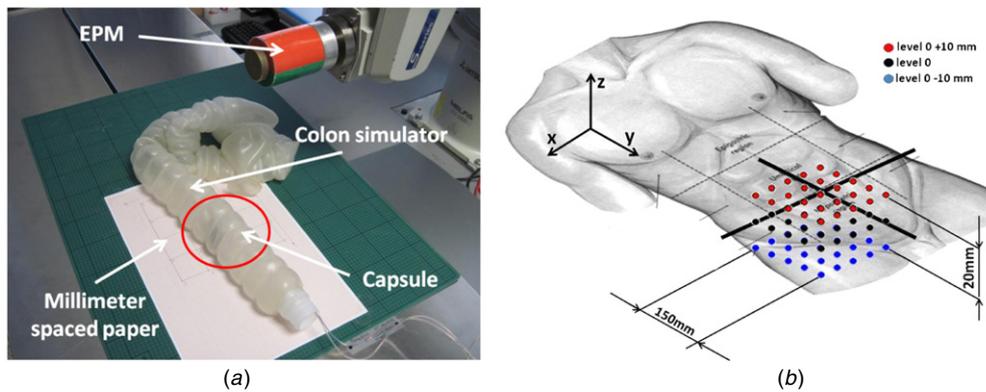

Figure 9. (*a*) Experimental set-up for evaluating localization procedure accuracy and (*b*) the schematic of the 75 measurements at three different heights.

end if
end while
$capsule location = mean(intersection 123)$.

   More information about MATLAB syntax, *find* and *intersect* functions, can be found in [28]. In order to validate the localization procedure in terms of accuracy, it was performed placing the capsule in 25 positions uniformly distributed on a surface comparable to an abdominal quadrant (150 mm × 150 mm) with an EPM-capsule distance half way between Hmin and Hmax. Each capsule position was referred to by positioning the device into a colon simulator and placing it on graph paper which was fixed on the reference plane (figure 9(*a*)). To perform a height dependence sensitivity analysis, the tests were repeated at two different heights, i.e. ±10 mm away from the initial localization height along the *Z* axis (figure 9(*b*)). As regards the analysis of results, average computational time and a successful localization parameter for the three localization levels were calculated for each procedure. This allowed us to select the algorithm optimizing the compromise between localization effectiveness and computational time. The capsule is considered linked if the EPM is located on the capsule. That happens if the effective capsule position belongs to the projection of the

EPM on the *XY* plane (successful target area). The successful localization parameter was defined as the percentage of times, with respect to the 25 measurements, the calculated point belongs to a successful target area centered in the effective capsule position. Once the best algorithm was identified, the deviation distribution between the real and the calculated points was estimated in the *X*, *Y* and *Z* directions, in order to evaluate technique accuracy.

3.4. Computational cost

The main advantage of this technique is that it is based on simple search algorithms applied to pre-calculated matrices obtained from a highly detailed analytical solution. The analytical magnetic field for the EPM was calculated on a wide domain of 400 mm in *X*, 800 mm in *Y* and 800 mm in *Z*, discretized in 5 mm distance points and generating for each component a matrix composed of 2.1 million elements. This huge number of data, which took quite a long time to calculate (174 min), was stored in memory and the intersection of iso-magnetic field module clouds of points was executed by applying simple translations and searching operations to the presented matrices. This approach offers the advantage
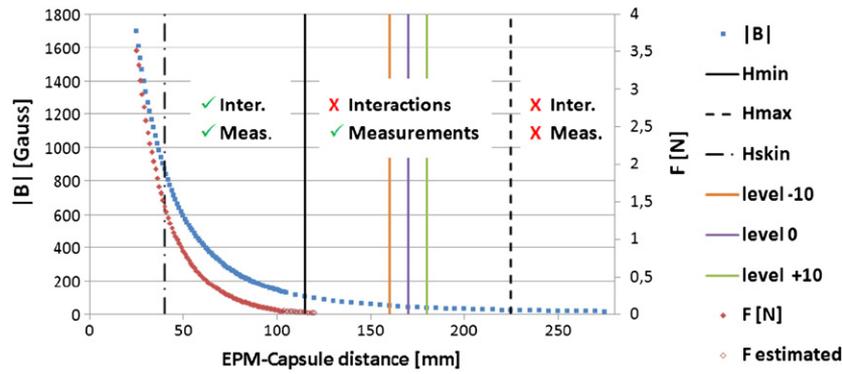
Figure 10. Plot of the magnetic field module and attraction force with respect to the EPM-capsule distance with operating ranges.
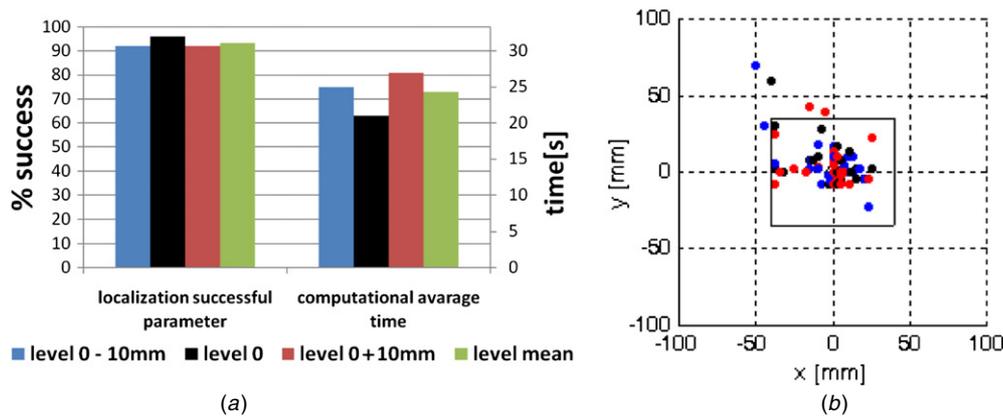

Figure 11. (*a*) Bar chart of the successful localization parameter and average computational time and (*b*) MATLAB screenshot of the calculated localization points belonging to the successful target area (in blue, black and red, respectively, the lower, medium and higher levels).

of minimizing computational cost while maintaining a high detail model that considers the actual features of the magnetic field generated by the permanent magnets. In addition, the magnetic fields resulting from the presence of two or more magnets in a domain of interest can be easily calculated by combining different pre-calculated solutions and applying spatial transformations to the matrices. For the selected application, the parameters of domain extension and spatial sampling were chosen to satisfy the need for a large workspace (the capsule was located in the lower abdomen with an approximate volume of 300 mm × 300 mm × 200 mm) and sensor accuracy (measurements of the magnetic field components were considered as performed at an infinitesimal point, while the sensors were fixed to a 5 mm plastic cube; a more refined spatial sampling than the cube dimension would be of no use).

4. Results and discussion

Experimental tests on the localization distance set the lower and upper limits for the localization range equal to 115 (Hmin) and 225 mm (Hmax), respectively (figure 10). Level 0, as defined above, is 170 mm. The localization procedure was also performed at 180 mm (level 0 + 10 mm) and at 160 mm (level 0 − 10 mm) from the capsule in order to quantify height dependence sensitivity. All algorithms were

processed by the MATLAB routines for the three different heights in each localization procedure, using the collected magnetic field modules as input. Average computational time and the successful localization parameter were calculated for each algorithm, thus allowing the most effective one to be identified (ranges of 16–149 s and 80–93%, respectively, for all algorithms). For brevity, only the results obtained with the best performing algorithm (second algorithm: 'if three or more values are over the threshold, then the algorithm considered the three highest measurements; otherwise it considered the four highest measurements') are reported in this paper. Average computational time and percentage of success are shown in figure 11(*a*) for the three localization levels and as a mean value for the three different heights. A MATLAB screenshot of the calculated localization points belonging to the successful target area is reported in figure 11(*b*).

The selected algorithm guarantees reliable localization of the capsule (successful localization parameter higher than 92%) within a short time (elaboration time less than 27 s) for all three different heights. It is worth mentioning that the successful localization parameters for the three localization levels differ from each other by less than 5%, thus confirming that the proposed technique is not significantly affected by initial height within the localization range. Due to this negligible difference and in order to improve statistical significance, the mean and maximum

position error between the real and analytically measured points and the deviation distributions for the selected algorithm in the *X* and *Y* directions were calculated considering all 75 tests. The deviation distributions between calculated and real points were -3.2 ± 18 mm in *X*, 5.4 ± 15 mm in *Y* and -13 ± 19 mm in *Z*. Therefore, efficiency results show that the capsule can be localized with an average position error of 14 mm along the *X* axis and 11 mm along the *Y* axis with an accuracy comparable to the EPM projection on the abdominal surface (± 35 mm along the *X* axis and ± 30 mm along the *Y* axis). The maximum errors, obtained without considering outliers, were 37.5 and 22.5 mm, respectively, for the *X* and *Y* axes. Mean and maximum errors were also calculated for the *Z* direction for the three different localization heights, although accuracy along this axis is not strictly significant for the current application. The algorithm showed its worst performance along this direction (mean and maximum position error equal to 19 and 57 mm, respectively), potentially due to small interaction movements of the capsule along *Z* during EPM localization measurements.

5. Conclusion and future work

The goal of the proposed work was to develop a reliable discrete-time localization algorithm compatible with magnetic locomotion in order to obtain the position of an endoscopic capsule and to establish (or re-establish) an effective magnetic link during GI examination. This innovative approach involves the use of magnetic sensors on board the capsule for localization purposes in magnetic-driven slide locomotion. In order to implement the localization procedure, analytical magnetic models of the IPM and EPM were developed. Once the model was defined and accurately validated, the localization algorithm was implemented and an experimental validation session was performed to assess the accuracy of the triangulation strategy. The position errors of 14 mm along the *X* axis, 11 mm along the *Y* axis and 19 mm along the *Z* axis were obtained with an elaboration time less than 27 s. Therefore, the proposed localization strategy represents an innovative tool for endoscopic capsule procedures where magnetic locomotion is used to control the device. The limitations in accuracy and calculation time of this procedure come from the wide workspace considered in this application, while the low spatial accuracy of magnetic field measurements is mainly due to the sensor size. Future improvements will include the implementation of a real-time localization strategy by adding magnetic field sources. It will be based on the same method exploited in this application, in which both the position and orientation of the capsule may be identified. In this case, the domain will be restricted to a region of interest and localization speed will significantly increase. The magnetic sensing module will be miniaturized by mounting the monoaxial sensors as bare silicon dies in a custom tridimensional system on package. Moreover, after miniaturizing the magnetic sensing module, it will be possible to use a higher spatial resolution for the analytical model in order to increase technique accuracy. As the last step, implementation in a compiled programming language connected to the robot control algorithm will complete the platform software.

References

[1] Iddan G J and Swain C P 2004 History and development of capsule endoscopy *Gastrointest. Endosc. Clin. N Am.* **14** 1–9
[2] Ishiyama M, Sendoh K and Arai K I 2003 Fabrication of a magnetic actuator for use in a capsule endoscope *IEEE Trans. Magn.* **39** 3232–4
[3] Kim B, Lee S, Park J H and Park O 2005 Design and fabrication of a locomotive mechanism for capsule-type endoscopes using shape memory alloys (SMAs) *IEEE-ASME Trans. Mechatronics* **10** 77–86
[4] Toennies J L, Tortora G, Simi M, Valdastri P and Webster R J III 2010 Swallowable medical devices for diagnosis and surgery: the state of the art *J. Mech. Eng. Sci.* **224** 1397–414
[5] Valdastri P, Webster R J, Quaglia C, Quirini M, Menciassi A and Dario P 2009 A new mechanism for mesoscale legged locomotion in compliant tubular environments *IEEE Trans. Robot.* **25** 1047–57
[6] Olympus Endocapsule, www.olympus-europa.com/endoscopy/
[7] Wakefield G M 2004 Magnetically propelled capsule endoscopy *US Patent US2004 199 054*
[8] Ciuti G, Valdastri P, Menciassi A and Dario P 2010 Robotic magnetic steering and locomotion of capsule endoscope for diagnostic and surgical endoluminal procedures *Robotica* **28** 199–207
[9] Carpi F and Pappone C 2009 Magnetic maneuvering of endoscopic capsules by means of a robotic navigation system *IEEE Trans. Biomed. Eng.* **56** 1482–90
[10] Ciuti G, Donlin R, Valdastri P, Arezzo A, Menciassi A, Morino M and Dario P 2010 Robotic versus manual control in magnetic steering of an endoscopic capsule *Endoscopy* **42** 148–52
[11] Kratochvil B E, Borer R, Sengul A, Kummer M P, Abbott J J and Nelson B J 2010 Octomag: an electromagnetic system for 5-dof wireless micromanipulation *IEEE Trans. Robot.* **26** 1006–17
[12] Choi H, Choi J, Jeong S, Cha K, Park J, Yu C, Kim J and Park S 2010 Novel electromagnetic actuation system for three-dimensional locomotion and drilling of intravascular microrobot *Sensors Actuators* **161** 297–304
[13] Fountain T W R, Kailat P V and Abbott J J 2010 Wireless control of magnetic helical microrobots using a rotating-permanent-magnet manipulator *IEEE Int. Conf. on Robotics and Automation (ICRA)* pp 576–81
[14] Fischer D, Schreiber R, Levi D and Eliakim R 2004 Capsule endoscopy: the localization system *Gastrointest. Endosc. Clin. N. Am.* **14** 25–31

[15] Thomas S 2006 Smart-pill redefines 'noninvasive' *J. Buffalo Physician* **40** 13–4

[16] Jacob H, Levy D, Shreiber R, Glukhosky A and Fischer D 2002 Localization of the given M2A ingestible capsule in the given diagnostic imaging system *Gastrointest. Endosc.* **55** AB135

[17] Wang X, Meng M and Hu C 2006 A localization method using 3-axis magnetoresistive sensors for tracking of capsule endoscope *Proc. IEEE/EMBS* pp 2522–25

[18] Hu C, Meng M and Mandal M 2006 The calibration of 3-axis magnetic sensor array system for tracking wireless capsule endoscope *IEEE/RSJ Int. Conf. on Intelligent Robots and Systems (IROS)* pp 162–67

[19] Yang W, Hu C, Meng M, Song S and Dai H 2009 A six-dimensional magnetic localization algorithm for a rectangular magnet objective based on a particle swarm optimizer *IEEE Trans. Magn.* **45** 3092–99

[20] Guo X, Yan G and He W 2009 A novel method of three-dimensional localization based on neural network algorithm *J. Med. Eng. Technol.* **33** 192–8

[21] Hong Y-S, Kim M-G and Lim E-J 2010 Position and orientation detection of capsule endoscopes in spiral motion *Int. J. Precis. Eng. Manuf.* **11** 31–7

[22] Rey J F *et al* 2010 Feasibility of stomach exploration with a guided capsule endoscope *Surg. Endosc.* **42** 541–5

[23] Stratton A 1941 *Electro-magnetic Theory* (New York: McGraw-Hill)

[24] Furlani E P 2001 *Permanent Magnet and Electromechanical Devices* (New York: Academic)

[25] Furlani E P, Reznik S and Janson W 1994 A three-dimensional field solution for bipolar cylinders *IEEE Trans. Magn.* **30** 5

[26] Furlani E P and Knewtson M A 1997 A three-dimensional field solution for permanent magnet axial field motors *IEEE Trans. Magn.* **33** 7

[27] Song C, Alijani A, Frank T, Hamma G B and Cuschieri A 2006 Mechanical properties of human abdominal wall measured *in vivo* during insufflation for laparoscopic surgery *Surg. Endosc.* **20** 987–90

[28] MATLAB User's Guide, http://www.mathworks.com/help/techdoc/